FOREX Publication
Open Access | Rapid and quality publishing

International Journal of
Electrical and Electronics Research (IJEER)
Research Article | Volume 14, Issue 2 | Pages 446-457 | e-ISSN: 2347-470X

Intelligent Capacitor Selection and Analysis for Self-Excited Reluctance Generator under Variable Conditions

Rewan M. Abo Elwafa[1*], M. Elwany[2], and A. B. Kotb[3]

[1]Electrical Power and Machines Dept., Institute of Aviation Engineering and Technology, Egyptian Aviation Academy, Ministry of Civil Aviation, Imbaba Airport, Giza, Egypt; Email: rewanmohamad63@gmail.com*
[2]Department of Elect. Eng. Faculty of Eng. Al-Azhar University, Cairo, Egypt; Email: MahmoudHosain1712.el@azhar.edu.eg
[3]Department of Elect. Eng. Faculty of Eng. Al-Azhar University, Cairo, Egypt; Email: moabdelsamie45@yahoo.com

***Correspondence:** *Rewan M. Abo Elwafa, rewanmohamad63@gmail.com*

ABSTRACT- This manuscript provides an analysis of a wind-driven self-excited reluctance generator (WDSERG) performance running under variable load conditions while maintaining a regular output voltage, and designs an Artificial Neural Network (ANN) model to forecast the value of the excitation capacitance required to maintain a WDSERG's generated voltage within desired bounds. The self-excited reluctance generator (SERG) has advantages over the induction generator (IG), which include steady frequency regardless of load or capacitance variation with proper performance. The analysis of steady-state for the reluctance generator (RG) is conducted according to d-q axes transformation. The suitable capacitance is determined for varying operating conditions to meet the main requirements for a loaded RG at constant voltage. To provide guidelines for designers, the variations of the capacitance corresponding to any change in the load impedance, power factor and prime mover speed are determined. The predicted excitation capacitance values that required to keep the generated voltage at a preferred constant level of 1± 0.1 pu under inputs condition. For example, at conditions (ZL (load impedance) =3pu (per unit), PF (power factor) =1, and constant speed) the capacitance 16.5275 μF (micro farad) make voltage constant at 1pu. It investigates how changing machine parameters affects the generator's performance and presents the speed above which excitation is not possible. Simulation results are supported through MATLAB coding analysis. This paper demonstrates the feasibility of steady voltage operation under in a variable load for SERG, presenting insights for practical implementation in standalone wind energy systems.

Keywords: Self-excited reluctance generator, Variable wind speed, Excitation Capacitance, Variable load, Artificial Neural Network, Evaluation metrics.

ARTICLE INFORMATION
Author(s): Rewan M. Abo Elwafa, M. Elwany, and A. B. Kotb;
Received: 02/09/25; **Accepted**: 01/05/26; **Published**: 25/06/26;
E- ISSN: 2347-470X;
Paper Id: IJEER 0209A06;
Citation: 10.37391/ijeer.140221
Webpage-link:
https://ijeer.forexjournal.co.in/archive/volume-14/ijeer-140221.html

Publisher's Note: FOREX Publication stays neutral with regard to jurisdictional claims in Published maps and institutional affiliations.

1. INTRODUCTION

With the worldwide shift toward sustainable energy resources, wind energy has emerged as one of the most promising and widely adopted form of renewable power. Its availability, scalability, and decreasing cost make it an excellent solution for both grid- connected and stand-alone application [1], [2]. In stand-alone or remote settings, such as rural communities, island systems, and agricultural zones, ensuring a reliable and efficient power supply is critical. This is where the role of green electrical generators becomes imperative to the performance of wind power systems. Designed for wind energy conversion, Permanent Magnet Synchronous Generators (PMSG) have garnered significant interest. They can be utilized directly or in conjunction with single or multi-stage gear box [3]-[6]. The permanent magnet in the PMSG rotor provides low rotor thermal stress, high torque density, and excellent energy conversion efficiency [7], [8]. However, the primary drawbacks of PMSG include high permanent magnet costs, cogging torque effects, and demagnetization of the permanent magnet material at high temperatures [9]. The implementation and design of the Doubly-Fed Induction Generator (DFIG) is considered a compelling option for variable speed constant frequency Wind Energy Conversion Systems (WECS) due to its substantial benefits [10], [11]. DFIG is capable of generating two outputs *via* the rotor and stator, needing smaller filters and converters, and eliminating the need for external reactive power compensation thanks to flexible excitation *via* the rotor circuit [12]. However, regular maintenance is necessary since the DFIG rotor has sliding rings and brushes. As a result, using DFIG for faraway and remote applications becomes less reliable and more expensive [9],[13]. Moreover, high complexity, large size, and cost of DFIG control and design make it unsuitable for small stand-alone, low-cost applications [9]. Self-Excited Induction Generators (SEIG) are preferred over traditional synchronous generators in standalone wind energy technologies because of the following benefits: They provide self-protection against short-circuit and high overload situations, and their brushless and durable design results in comparatively inexpensive initial and maintenance costs [14].

FOREX Publication
Open Access | Rapid and quality publishing
International Journal of Electrical and Electronics Research (IJEER)
Research Article | Volume 14, Issue 2 | Pages 446-457 | e-ISSN: 2347-470X

The facility of the SEIG to transform energy from mechanical to electrical across a large speed range has made it a good candidate to replace synchronous machine in different applications [15]. However, the machine is impacted by variation in voltage and frequency with a change in load, which is an inherent problem, and its correction requires complex technology. Another kind of generator that provides additional advantages is the Self Excited Reluctance Generator (SERG), which is a synchronous machine with salient poles or a segmented rotor that doesn't need to be excited. The SERG is now popular because of its advantages over SEIG, such as fixed frequency, improved voltage regulation, and lower copper and iron losses. Considerable progress has been made in the design and analysis of SERG [16], and some authors have attempted to create an SERG equivalent circuit while ignoring the rotor saliency effect [17]. An Additional model comparable to a salient pole generator has been developed without field winding, utilizing Park's transformation as the basis for its analysis [18],[19]. Expressions under pure inductive loads and open circuit for cut-off speeds are obtained [20], while an IM with an axially laminated anisotropic rotor is used to create a laboratory model, as shown in [21]. A mathematical model based on d-q axes transformation is created, and some of the computed curves are compared with the corresponding experimental results [22]. In this paper, the performance based on steady state conditions of an isolated SERG under various operating situations has been studied using a simple method, and ANN model has been developed to automatically select the excitation capacitance value for specified operating conditions of wind speed, load impedance and power factor. These constitute the inputs to the ANN model and the output is the excitation capacitance value that is vital to achieving a controlled output voltage. The main goal of this work is to determine the suitable values of capacitance needed to obtain the rated voltage for different values of loads. The analysis is modified to be valid for the operation of SERG at any speed and load to achieve a constant voltage.

2. ANALYSIS OF WDSERG

2.1. Model of Wind Turbine System

A model for Wind Driven SERG (WDSERG) with adjustable excitation is shown in *figure 1*. The model consists of a prime mover represented by a wind turbine, a reluctance generator, a gearbox, and an excitation capacitance.

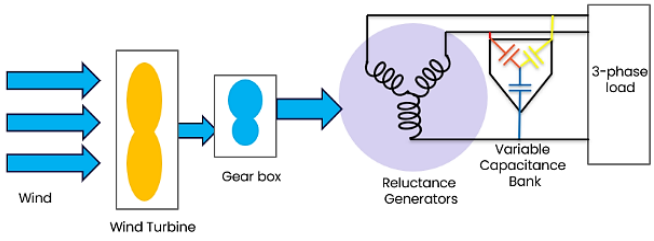

Figure 1. Model of WDSERG

The output mechanical power (in watts) of a wind turbine is represented as

$$P_t = \frac{1}{2} C_p(\lambda, \beta) \rho A V_W^3 \quad (1)$$

Where: C_p is the turbine's performance coefficient, λ is the ratio of tip speed (TSR), β is the angle of pitch for the blade, ρ is the density of air in kg/m3, A is the turbine swept area in m^2, and V_W is the speed of wind in m/s. The turbine's performance coefficient (Cp) is a function of pitch angle of the blade (β) and tip speed ratio (λ) as described in [23].

$$C_p(\lambda, \beta) = C_1 \left(\frac{C_2}{\lambda_1} - C_3 \beta - C_4 \right) e^{\frac{-C_5}{\lambda_1}} + C_6 \lambda \quad (2)$$

Where:

The values of the coefficients, including C_1 to C_6 are defined as follows:

$C_1 = 0.5176; C_2 = 116; C_3 = 0.4; C_4 = 5; C_5 = 21; C_6 = 0.0068.$

and,

$$\lambda_1 = \frac{(\beta^3+1)(\lambda+0.08\beta)}{\beta^3 - 0.028\beta - 0.035\lambda + 1} \quad (3)$$

and the tip speed ratio is:

$$\lambda = \frac{\omega_t R_t}{V_w} \quad (4)$$

Where: ω_t is the tip speed of the rotor blade in rad/s, and R_t is the radius of the turbine blade.

The wind turbine's mechanical torque is expressed as follows:

$$T_t = \frac{P_t}{\omega_t} = \frac{0.5 C_p(\lambda,\beta) \rho A V_w^3}{\omega_t} \quad (5)$$

2.2. Phasor Diagram of SERG under Load

The phasor diagram of *figure 2*, is developed for a SERG, without damper windings, based on Park's *d-q* transformation connected to a variable load.

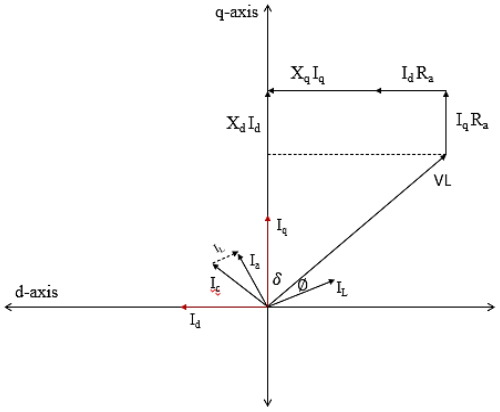

Figure 2. Phasor diagram of loaded SERG

3. MATHEMATICAL ANALYSIS FOR SERG WITH VARIABLE LOAD

The equation of voltage for the RG without the rotor conductor, with the terms of the field winding omitted [24]-[26] can thus be written as in *equations (6) to (11).*

FOREX Publication
Open Access | Rapid and quality publishing
International Journal of Electrical and Electronics Research (IJEER)
Research Article | Volume 14, Issue 2 | Pages 446-457 | e-ISSN: 2347-470X

The following assumptions have been made in this work:

1. Magnetic saturation only affects the d-axis magnetizing inductance.
2. The loss of core is negligible
3. The time harmonics and space harmonics in the air gap flux are negligible in the current wave forms and electromotive force.

From the phasor diagram of *figure 2*, the voltage can be obtained in terms of *d* and *q*-axes components and it may be given as:

$$V_d = -V_L \sin\delta = R_a I_d + X_q I_q \quad (6)$$

$$V_q = V_L \cos\delta = X_d I_d - R_a I_q \quad (7)$$

Where v_L is the terminal load voltage, R_a is the armature resistance and δ is the load angle in electrical degree. The direct and quadrature current components are given in terms of both load and excitation currents as follows:

$$I_d = I_C \cos\delta - I_L \sin(\delta + \varphi) \quad (8)$$

$$I_q = I_C \sin\delta + I_L \cos(\delta + \varphi) \quad (9)$$

The load current I_L lags the terminal voltage by an angle φ ,and the excitation current I_C leads the terminal voltage V_L by an angle $\pi/2$. The substitution of $I_L = V_L/Z_L$ and $I_C = V_L/X_c$ in equations (6,7,8,9) with some manipulations, the angle of load, δ can be obtained in terms of Z_L, φ, X_q, R_a and the capacitance based self-excitation C as follows:

$$\tan\delta = \frac{X_q \cos\emptyset - R_a \sin\emptyset + Z_L R_a / X_c}{X_q \sin\emptyset + R_a \cos\emptyset + Z_L[1 - X_q/X_c]} \quad (10)$$

where the load impedance $Z_L = \sqrt{R_L + X_L}$,$X_c = 1/\omega c$,and $\omega = 2\pi f$

The rated data utilized in this paper are demonstrated in *table 1*, as in the following:

Table 1. Main Parameters of the Reluctance Machine

Parameter	Value
Rated phase voltage(V_n)	220V
Rated frequency (f)	60 Hz
Rated current (I_n)	2.2A
Base impedance (Z_b)	100Ω
Stator winding resistance (R_a)	0.1 PU
unsaturated d-axis reactance(X_d)	3 PU
unsaturated q-axis reactance (X_q)	0.8 PU
base of relative speed (v_b)	1.0 PU
power factor	0.8 lagging

It is very important that, the study in this paper have been analyzed based on per unit system (PU), as a result, the figures are introduced based pu except that the excitation capacitance is used as its actual values in micro farad.

4. PERFORMANCE UNDER CONSTANT SPEED VARIABLE EXCITATION CAPACITANCE

The quantity of terminal capacitance, load current, power factor, and external drive speed all affect the generated voltage. The practical use of this concept in electric power generation has lately been actualized alongside the growing interest in wind energy as an alternative to non-renewable energy sources.

4.1. Effect of Variation Load on the Load Angle

The variation of the angle of load δ alongside the capacitance based on self-excitation *C* in case of variable impedance of load, the angle of load δ rises as the capacitance of self-excitation *C* rises getting a certain value, see *figure 3(a)&(b).*

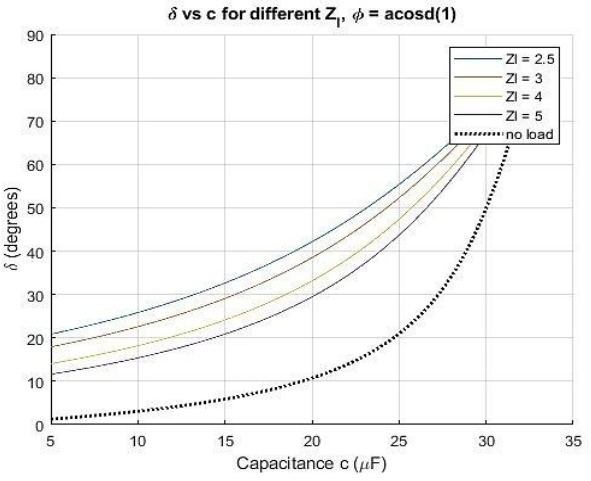

(a)

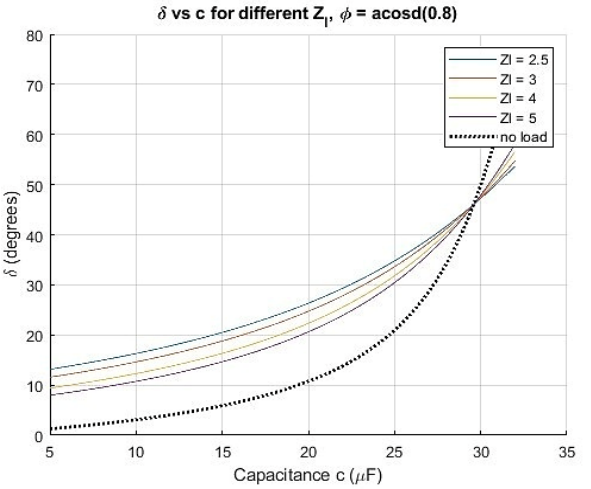

(b)

Figure 3. Excitation capacitance versus δ in case of (a) unity PF (b) 0.8 PF lag

4.2. The Variation of Direct Axis Magnetizing Reactance X_d with Load

The X_d can be obtained from *equation (7)* as in the following equation in *eq. (11)*:

FOREX Publication
Open Access | Rapid and quality publishing
International Journal of Electrical and Electronics Research (IJEER)
Research Article | Volume 14, Issue 2 | Pages 446-457 | e-ISSN: 2347-470X

$$X_d = \frac{Z_L + R_a \cos\emptyset + [(Z_L/X_c) - \sin\emptyset]\, R_a \tan\delta}{(Z_L/X_c) - \sin\varphi - \cos\varphi \tan\delta} \quad (11)$$

At a fixed speed, as depicted in *figure 4(a)* and *(b)*, the variation of X_d with excitation or compensating capacitance initiates at its value of unsaturation and falls until its extents or reaches a certain and defined minimum value. By way of the capacitance C increases additional, the *d*-axis reactance steadily growths again, approaching a value close to the machine's unsaturated reactance. For each load value there are two values of X_d, which define as the possible range of self-excitation capacitance (C). Thes two distinct values of C, including C_{min} and C_{max} are defined as the cut in and cut off capacitance, respectively. The simulation results present that the operation range of the machine is comparatively wide at light load and the range is narrow at operation-based full load.

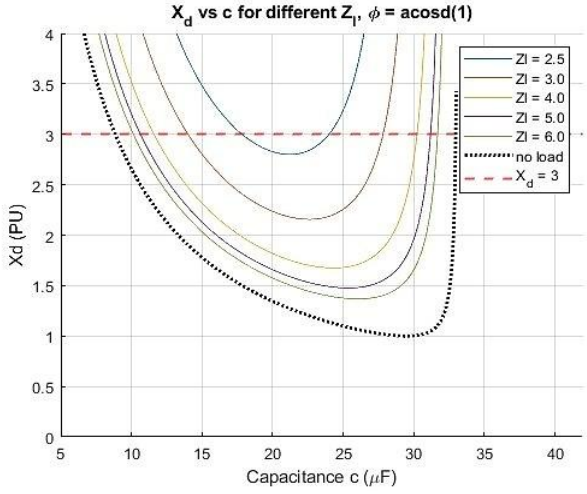

(a)

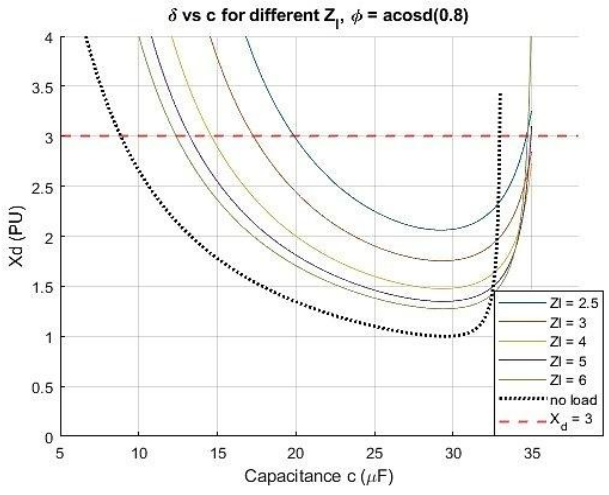

(b)

Figure 4. Excitation capacitance versus Xd in case of (a) unity PF (b) 0.8 PF lag

4.3. The Variation of Terminal Voltage V_L with Load

Utilizing the aforementioned analytical technique, an appropriate computation is conducted to examine the performance-based on steady-state condition for the isolated RG under diverse loads. The curve of *d*-axis saturation is characterized by fitting approach [27] to give the direct current as function of the direct reactance shown in *figure 5*. It is evidenced that the RG will fail to excite if the state of operation needs a value of X_d larger than the unsaturated reactance of the- machine. The modeled function is depicted as in following equation;

$$I_d = 0.09517X_d^4 - 0.9662X_d^3 + 3.835X_d^2 - 7.111X_d + 5.603 \quad (12)$$

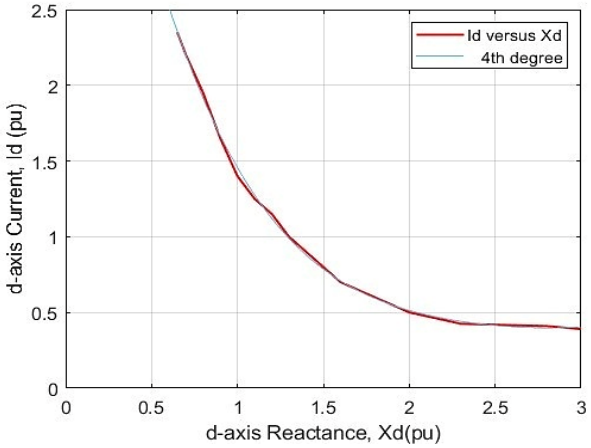

Figure 5. Direct axis magnetizing curve for the specified reluctance generator

Also, I_d can be given grom *equation (8)* in the form:

$$I_d = V_L \frac{(Z_L/X_c)\cos\varphi - \sin(\varphi + \delta)}{Z_L} \quad (13)$$

Then, the load voltage VL can be expressed in the form:

$$V_L = I_d \frac{Z_L}{(Z_L/X_c)\cos\delta - \sin(\varphi+\delta)} \quad (14)$$

The variant of V_L in relation with the used capacitance for excitation C at constant speed and for various impedance values for load, see *figure 6(a)* and *6(b)*.

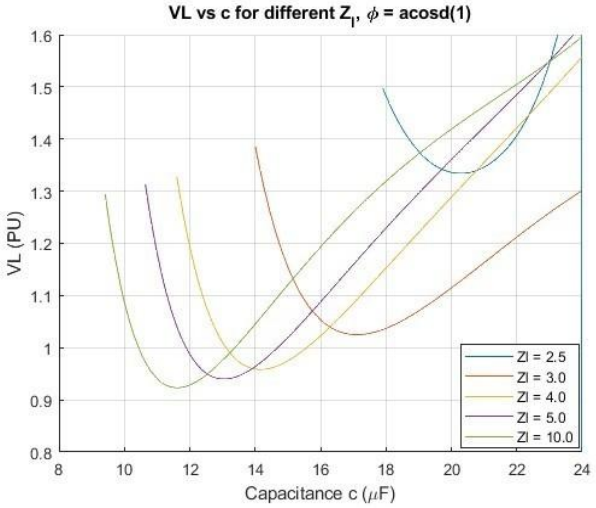

(a)

FOREX Publication
Open Access | Rapid and quality publishing
International Journal of Electrical and Electronics Research (IJEER)
Research Article | Volume 14, Issue 2 | Pages 446-457 | e-ISSN: 2347-470X

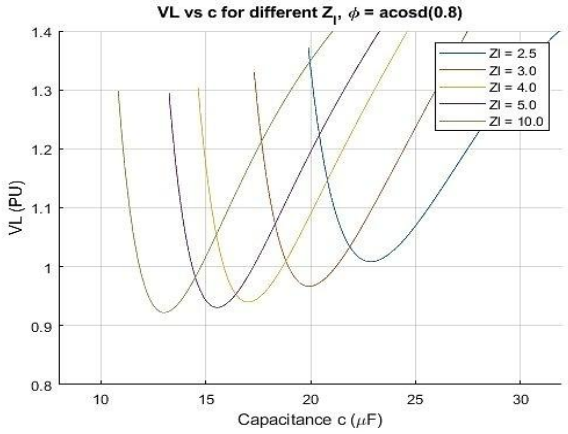

(b)

Figure 6. Excitation capacitance against V_L in case of (a) unity PF (b) 0.8 PF lag

The excitation *C* rises the V_L decreases at constant excitation *C* and form this is value the excitation capacitance increases the V_L rises attainment its maximum number at the end of the range of excitation. The excitation *C* initially causes a decrease in terminal voltage at a constant excitation capacitance value; beyond this point, an increase in excitation capacitance results in an increase in terminal voltage, peaking at the conclusion of the excitation range. It is clear that the generator outside this value of *C* does not work and consequently the V_L drops to *zero*.

4.4. Effect of Variation Impedance Load on the load and currents of capacitor

The other RG performance factors, such load and capacitor currents, can be ascertained if V_L is known.

$$I_L = \frac{V_L}{Z_L} \tag{15}$$

$$I_c = V_L\, \omega\, c \tag{16}$$

The variation of the load current I_L and the excitation current *Ic* against the excitation capacitance C, Both the excitation currents and load rise as the capacitor of self-excitation is increased, see *figure 7(a)&(b)* and *figure 8(a)&(b)*. This occurs due to the rise in self-excitation frequency.

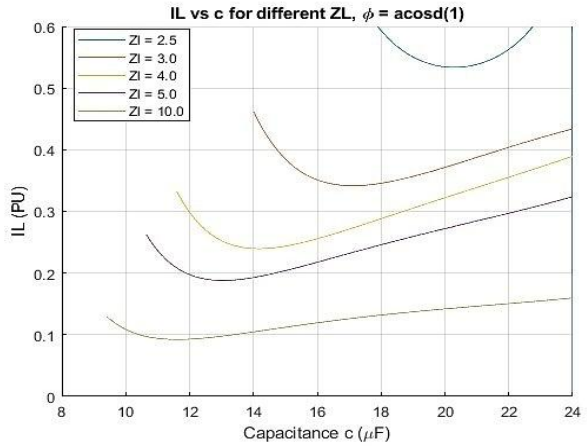

(a)

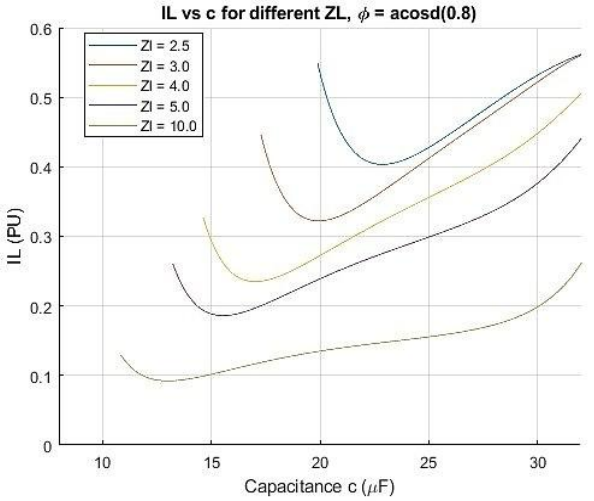

(b)

Figure 7. Variation of load current with excitation capacitance (a) unity PF (b) 0.8 PF lag

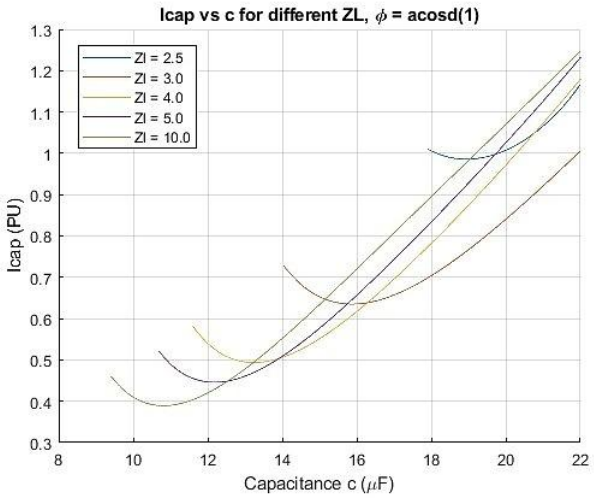

(a)

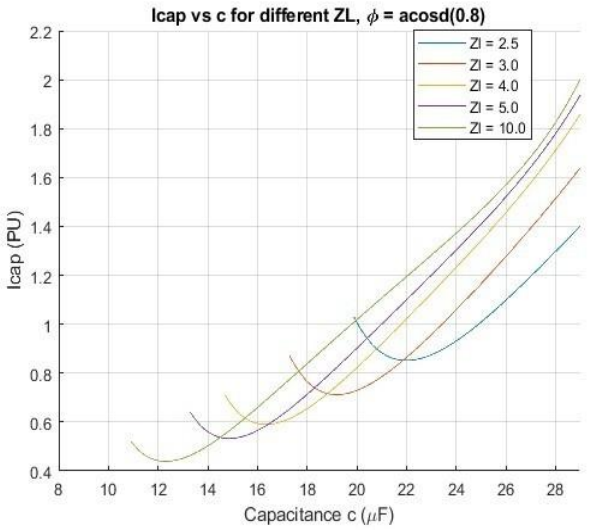

(b)

Figure 8. Excitation capacitance against current capacitor at (a) unity PF (b) 0.8 PF lag

FOREX Publication
Open Access | Rapid and quality publishing
International Journal of Electrical and Electronics Research (IJEER)
Research Article | Volume 14, Issue 2 | Pages 446-457 | e-ISSN: 2347-470X

5. PERFORMANCE OF SERG WITH VARIABLE SPEED

In our application, the prime mover speed (a) of the SERG will be changed according to the wind speed variation. This gives the per unit speed, more or less than the unity where a = n/ns. Accordingly, the generated voltage and the reactance of the generator circuit will also vary.

5.1. Effect of speed Variation on the Load Angle

The effect of the speed variation could be considered for the load angle (δ) by substituting aX_{L} , aX_{d} , $aX_{\mathrm{q}}$and $a\omega c$ for X_{L}, X_{d}, X_{q} and ωcrespectively. Accordingly, *eq. (10)* may be modified as in the following mathematical relation;

$$tan\ \delta = \frac{a[X_q R_L - R_a X_L + (R_L^2 + a^2 X_L^2) R_a \omega\, c}{R_a R_L + R_L^2 + a^2 (X_q X_L + X_L^2 - R_L^2 X_q \omega\, c - a^2 X_L^2 X_q \omega\, c)} \quad (17)$$

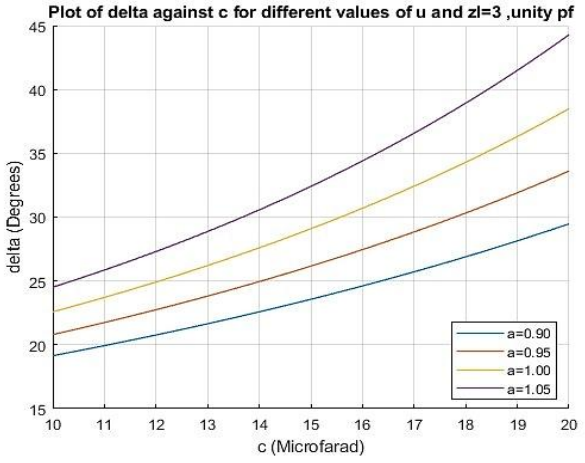

(a)

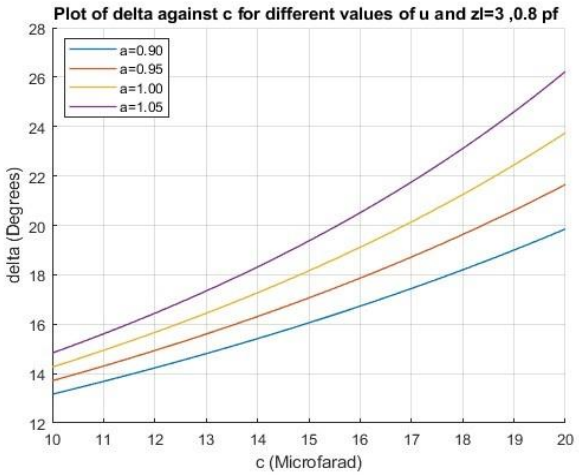

(b)

Figure 9. Excitation capacitance against δ at (a) unity PF (b) 0.8 PF lag

The value of δ such as increases with the increasing of the speed value at the same excitation capacitance value. Also, the used capacitance for self-excitation should be increased to recompense the speed decreasing effect for a certain load angle, see *figure 9(a)&(b)*.

5.2. The Variation of Direct Axis Magnetizing Reactance X_d with Speed

In case of variation of speed, X_d can be represented mathematically using the following relation by modifying *eq. (11)*;

$$\mathrm{X_d} = \frac{\mathrm{R_L^2 + R_a R_L + a^2 X_L^2 + [(R_L^2 + a^2 X_L^2)\omega\, c - X_L] a R_a \tan\delta}}{\mathrm{a^2\, \omega\, c(R_L^2 + a^2 X_L^2) - a^2 X_L R_L \tan\delta}} \quad (18)$$

Besides, in case of variable speed, as depicted in *figure 10*, the variation of X_d with excitation capacitance C.The variation of X_d with excitation capacitance at a given speed shows that as the excitation capacitance increases, X_d decreases from its unsaturated value until it reaches a minimum point. When the speed is reduced, X_d gradually rises again, approaching the unsaturated reactance of the SERG.

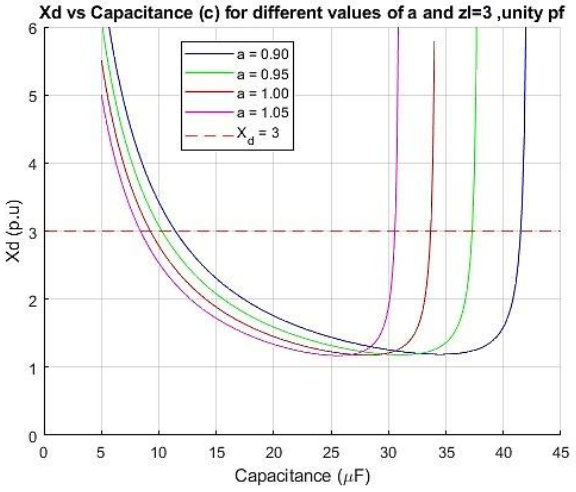

(a)

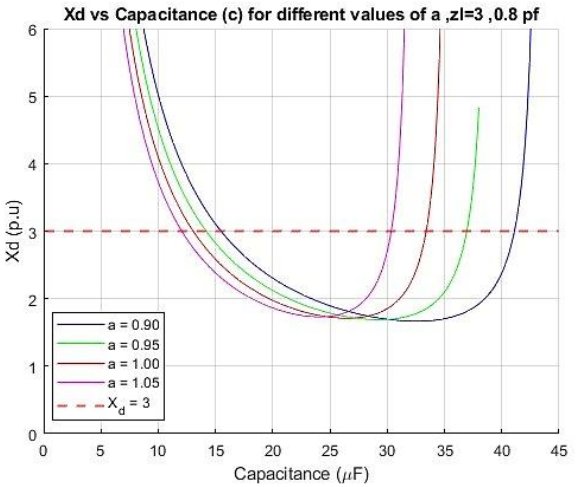

(b)

Figure 10. Excitation capacitance against magnetizing reactance at (a) unity PF (b) 0.8 PF lag

To determine the range of capacitance that allows self-excitation, the minimum and maximum capacitance values referred to as the cut in and cut off capacitances, respectively must be specified.

FOREX Publication
Open Access | Rapid and quality publishing
International Journal of Electrical and Electronics Research (IJEER)
Research Article | Volume 14, Issue 2 | Pages 446-457 | e-ISSN: 2347-470X

5.3. The Variation of Terminal Voltage V_L with Load

At speed variation, V_L can be expressed mathematically using the following relation by modifying *eq. (14);*

$$V_L = I_d \frac{(R_L^2 + a^2 X_L^2)}{(R_L^2 + a^2 X_L^2)a\omega c \cos\delta - aX_L \cos\delta - R_L \sin\delta} \quad (19)$$

Figure (a)&(b), illustrates the variant of V_L in relation with the used capacitance for excitation C at variable speed.

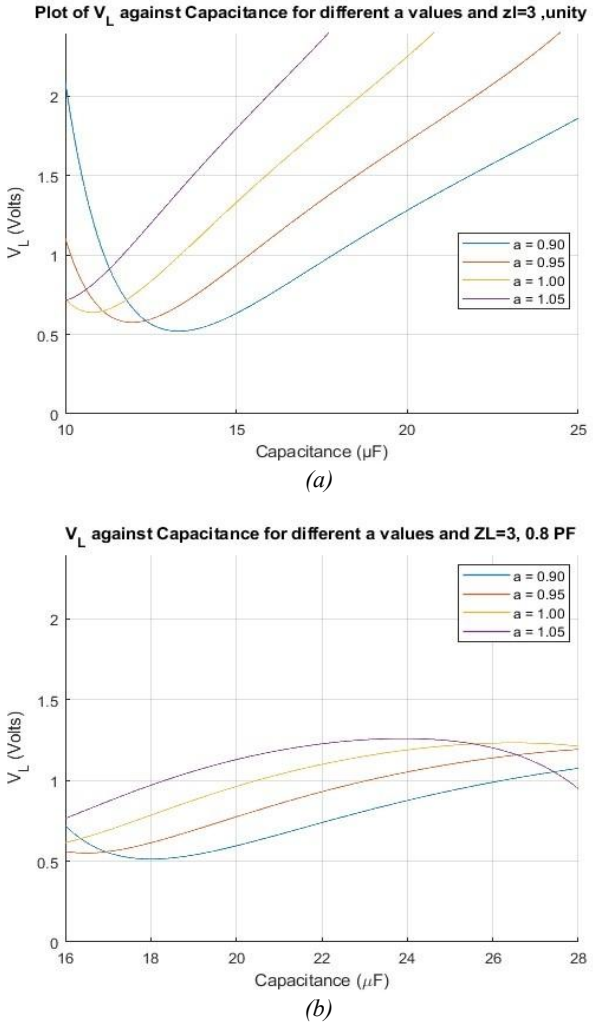

Figure 11. Excitation capacitance vs VL at (a) unity PF (b) 0.8 PF lag

The VL rises with an increase in speed of rotor as depicted in *figure 11*. For a constant speed, the terminal voltage also increases as the excitation capacitance C grows, up to the end of the excitation range. It can be noted that voltage build-up for a given C begins only after the rotor reaches a certain speed, known as the critical speed. Moreover, increasing the excitation capacitance reduces the value of this critical speed. The relationship between excitation C and rotor speed at different fixed terminal voltages is evaluated to ensure stable operation of the self-excited reluctance generator when connected to the main power grid. *Figure 12(a)&(b)*, clearly displays that, for a constant V_L, the required excitation capacitance decreases as the rotor speed increases.

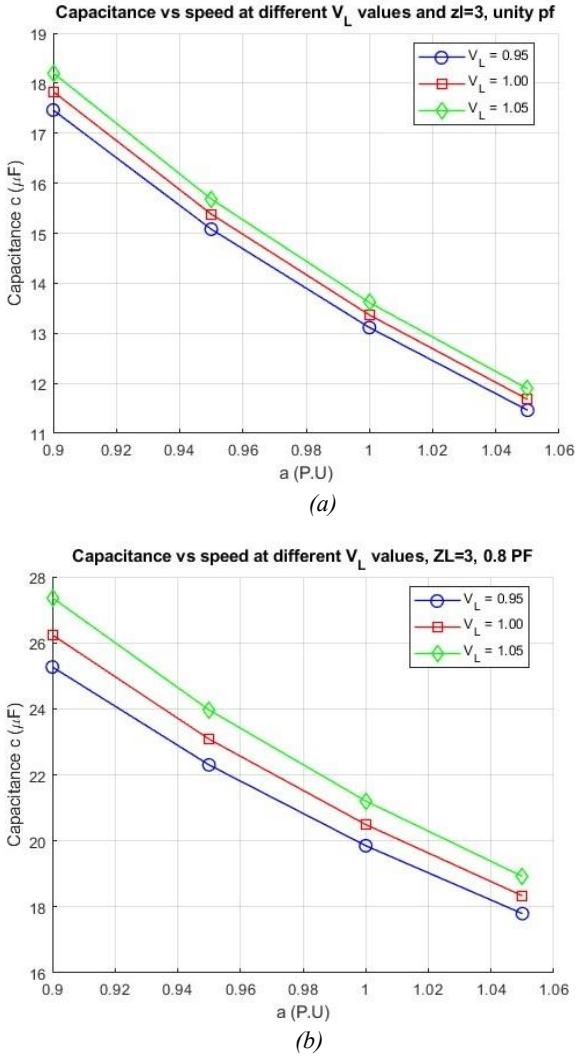

Figure 12. The excitation capacitance against Vs speed at (a) unity PF (b) 0.8 PF lag

The capacitance range needed to sustain a constant VL, across a given speed variation under different load conditions as presented in *figure 12(a)&(b)*. It is evident that the self-excitation capacitance need to sustain VL=1 PU (for example) during speed changes from (0.95 PU to 1.05 PU), without a noticeable change in machine frequency, It is necessary to modify the excitation capacitance from 17.833 μF to 11.679 μF approximately at Z_L=3 and unity power factor, see *figure 12(a)*, and approximately from 26.241μF to 18.333μF at Z_L=3 and 0.8 power factor, see *figure 12(b)*. Likewise, to keep the output voltage between 1.05 P.U. and 0.95 constant.

6. CAPACITANCE ESTIMATION BASED ON ARTIFICIAL NEURAL NETWORK (ANN)

Artificial Neural Networks (ANNs) provide an alternative approach for handling both linear and nonlinear curve-fitting problems [28],[29]. They do not depend on an explicit dynamic model of the system, since they are capable of learning complex functional relationships and nonlinear interactions directly from data. In general, neural networks are

FOREX Publication
Open Access | Rapid and quality publishing
International Journal of Electrical and Electronics Research (IJEER)
Research Article | Volume 14, Issue 2 | Pages 446-457 | e-ISSN: 2347-470X

considered powerful approximation tools because they can model highly complicated functions regardless of whether the behavior is linear or nonlinear [28], [30]. For this reason, they are widely used in applications such as signal processing, pattern recognition, function approximation, and classification [31]–[34]. The artificial neuron is the core unit of an ANN and is designed to simulate the function of a biological neuron. The inputs are multiplied by adjustable weights, summed together, and then passed through a function to produce the output (see *figure 13)*.

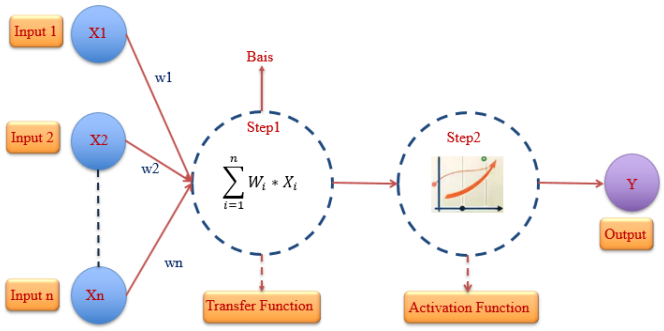

Figure 13. The artificial neuron model

7. RESULTS AND DISCUSSION

This section is divided into two scenarios, the first scenario discusses the traditional analysis for the proposed generator based on the mathematical equations that governing the system with simulation using MATLAB script, while the second scenario depicts the applying of ANN approach as intelligent technique to predict the suitable excitation capacitance for the proposed generator.

7.1. Scenario 1: Traditional Analysis

In this scenario, the discussion of the required excitation capacitance to guarantee the operating voltage at 1 pu is demonstrated based on numerical values and analysis process under variable conditions.

Table 2. Required capacitance at unity pu of operating voltage and unity pf

Zl	P.F	Delta (degree)		Xd (pu)		C_{min} (µf)	C_{max} (µf)	Vl (pu)
		at C_{min}	at C_{max}	at C_{min}	at C_{max}			
3	1	31.593	40.915	2.5634	2.1873	16.5275	21.0277	1
4		21.687	29.142	2.6308	1.9649	13.1711	18.0466	
5		17.342	23.573	2.6471	1.9136	12.0196	16.8380	
6		14.717	20.217	2.6539	1.891	11.4360	16.2049	
10		9.8568	14.025	2.6611	1.8636	10.5979	15.2425	

Table 2 show the capacitance need to satisfy the required operating voltage v=1 at unity power factor. There are two range of capacitance C_{min} (minimum value) and C_{max} (maximum value). Based on the analysis, the min values are chosen in case of the value of Xd under the unsaturated value (Xdunsaturated=3 pu).

Table 3. Required capacitance at unity pu of operating voltage and 0.8 pf

Zl	P.F	Delta(degree)		Xd(PU)		Cmin (µf)	Cmax (µf)	Vl (pu)
		at Cmin	at Cmax	at Cmin	at Cmax			
3	0.8	19.67	22.919	3.4375	2.6804	15.866	18.6668	1
4		15.735	18.744	3.0765	2.3939	14.3633	17.2696	
5		13.288	16.062	2.932	2.2795	13.4600	16.3948	
6		10.87	13.234	3.1771	2.4067	11.8478	14.7713	
10		7.577	10.959	3.0786	2.0394	10.598	15.243	

In *table 3*, the analysis show that the required capacitance to satisfy the required operating voltage *v*=1 at 0.8 power factor lagging. There are two range of capacitance C_{min} and C_{max} and it is recommended to choose the min one if the value of Xd under the unsaturated value (Xdunsaturated= 3 pu).

7.2. Scenario 2: Prediction of Capacitance based ANN

The ANN architecture based on multilayer perceptron is created, and real-time data is used to train the network. ANN models were developed as a substitute to enhance the estimate process. The neural network's inputs are load impedance (Z_L), load power factor (PF) and speed of wind (a) while the output is the estimated capacitance (C) (see). The model of ANN used a 694 sample for training process,149 sample for testing process, and 149 sample for validation process.

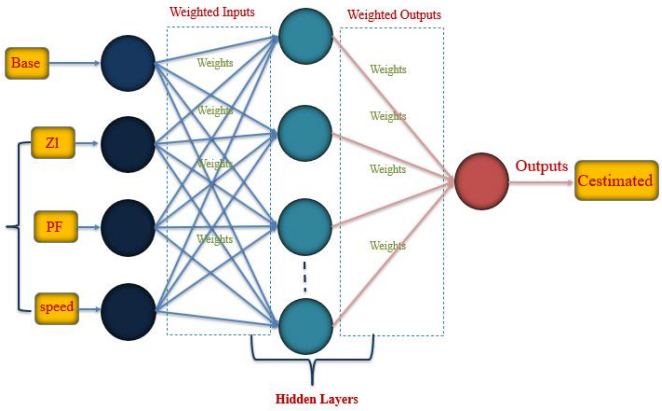

Figure 14. Schematic diagram for proposed ANN

Three kinds of ANNs Levenberg Marquardt (LM), Bayesian Regularization (BR), and Scale Conjugate Gradient (SCG) were trained using the system's collected data using ten hidden layers, see *figure 14*. The training data comes from the previously mentioned analytical findings. The evaluation of the suggested prediction ANN structure is tested using the two metrics: mean square error (MSE), and coefficient of determination (R^2) as shown in *eqs. (20), (21)*. These criteria are used to test the performance of ANNs. As well, the value of R^2 =1, shows an excellent fit and R^2 near 1 refer to a good fit. Consequently, it is very clear that the values of R^2 is proportional to the fitting quality.

FOREX Publication
Open Access | Rapid and quality publishing
International Journal of Electrical and Electronics Research (IJEER)
Research Article | Volume 14, Issue 2 | Pages 446-457 | e-ISSN: 2347-470X

$$\text{MSE} = \frac{1}{n}\sum_{i=1}^{n}(t_i - z_i)^2 \quad (20)$$

$$R^2 = 1 - \frac{\frac{1}{n}\sum_{i=1}^{n}(t_i - z_i)^2}{\frac{1}{n}\sum_{i=1}^{n}(t_i - t_{i-mean})^2} \quad (21)$$

Where, n is the number of samples, t_i is forecasting capacitance -based ANN, z_i represents actual collected capacitance, and t_{i-mean} is mean of predicting capacitance-based ANN. *Tables 1* show the evaluation performance for the proposed models of ANN in different criteria. Besides, *figure 15* demonstrates an evaluation performance in chart shape. In addition, *figure 16* demonstrates regression in training of ANN based on LM. The training performance for the LM is depicted in *figure 17*. The error histogram is given in *figure 18*. Besides, the training state for LM algorithm is shown in *figure 19*.

Table 4. Evaluation Performance of ANN Models

Methods	Training of ANN Model		Validation of ANN Model		Testing of ANN Model		prediction of ANN Model	
	R2	MSE	R2	MSE	R2	MSE	R2	MSE
LM	0.9490	0.6508	0.9570	0.5759	0.9541	0.6388	0.98218	0.13011
BR	0.9491	0.6516	Nan	Nan	0.9392	0.8225	0.96368	0.29752
SCG	0.9115	1.1135	0.9263	1.0563	0.9195	0.9473	0.9577	0.4669

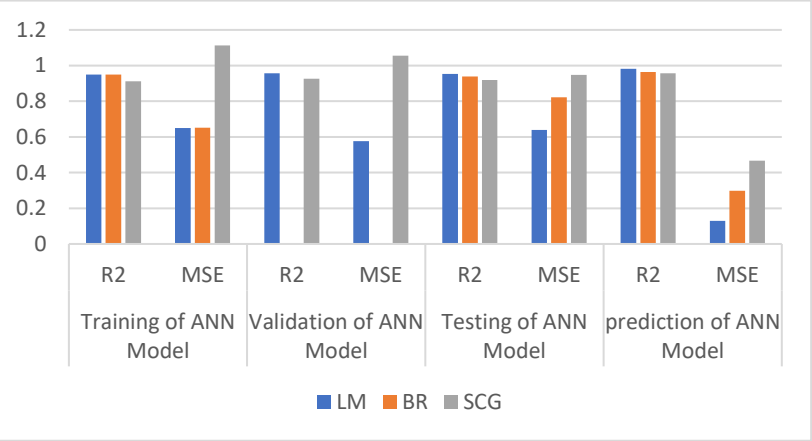

Figure 15. Comparison chart of various ANN Model

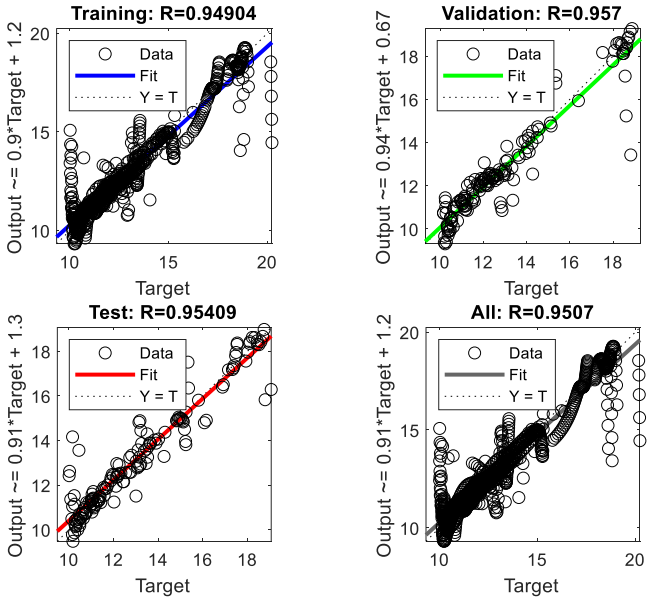

Figure 16. The ANN Regression plot performance

FOREX Publication
Open Access | Rapid and quality publishing
International Journal of Electrical and Electronics Research (IJEER)
Research Article | Volume 14, Issue 2 | Pages 446-457 | e-ISSN: 2347-470X

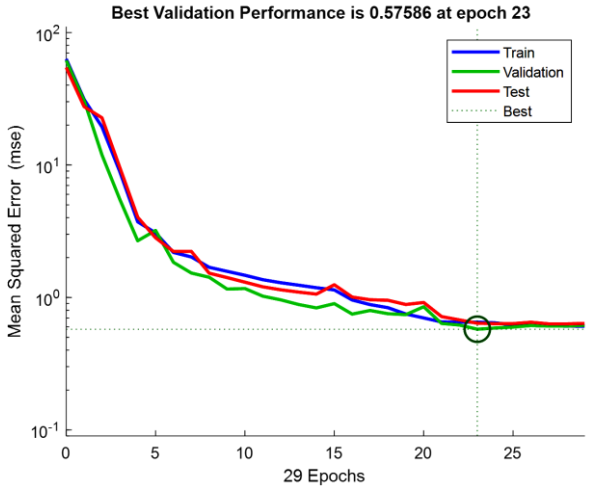

Figure 17. Best Training Performance for LM Algorithm

Figure 18. Error Histogram of LM Algorithm

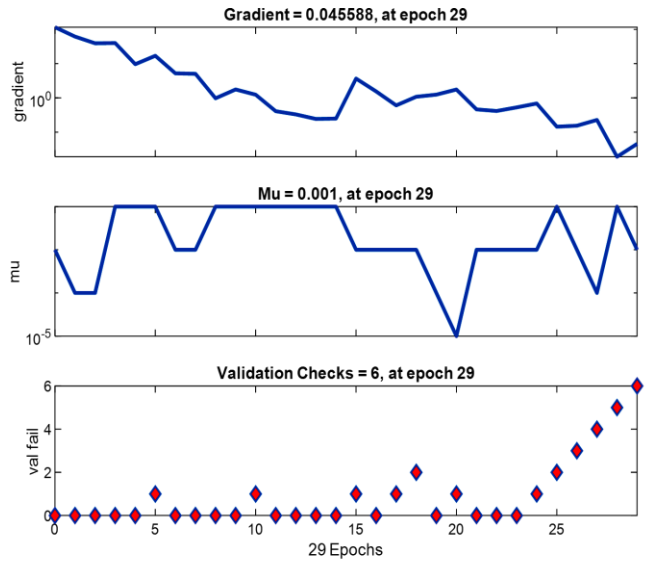

Figure 19. Training State of LM Algorithm

6. CONCLUSIONS AND FUTURE WORKS

The SERG has good regulation of voltage, fixed frequency and high efficiency regardless of the changes of load or variation in capacitance. The generator offers also suitable operating situations as a wind driven alternator, though, a converter of intermediate frequency is needed for supplying an isolated load. The required range of capacitance value for self-excitation which allows the generator terminal voltage to be constant for altered values of load, at any presented power factor. The forecasted excitation capacitance range that required to keep the generated voltage at a preferred constant level of 1± 0.1pu under inputs condition Z_L=3pu, PF=1, and speed not variated is 16.5275 to 21.077 µF make voltage constant at 1pu and at Z_L=3pu, PF=0.8, and speed not variated is 15.866 to 18.6686 µF. As the power factor decreases, the excitation capacitance must be increased to offset the inductive effects and supply the reactive power needed for the SERG's self-excitation. The analysis is extended and adapted to be usable with flexible speed and the capacitance range needed to maintain the terminal voltage constant via the speed variation is investigated. In this paper presents the SERG, designed to be powered by wind energy and integrated into the load. The excitation capacitance needs to be increased to counteract the impact of speed reduction at a given load angle, and the necessary excitation capacitance must be reduced as the prime mover speed increases in order to maintain a stable terminal voltage. The paper also introduces general guidelines for the designers which lead to a correct choice of direct and quadrature axes reactance as well as the armature resistance The mathematical analysis based on a *d-q* axes transformation is used. In this paper, three ANN models are built based on LM, SCG, and BR algorithms. The dataset of data is collected from the analysis. The three algorithms are compared based on different performance tests such as MSE and R2. LM is recommended as the best algorithm for the capacitance prediction. In future works, the researcher's efforts about this point shouldn't stop until the best results for choosing the optimal capacitance by using the artificial intelligence.

Supplementary Materials: The data are available upon request.

Author Contributions: "Conceptualization, R.M.AE., M.E and A.B.K.; methodology, R.M.AE and A.B.K; software, R.M.AE.; validation, M.E and A.B.K.; formal analysis, R.M.AE.; investigation, M.E and A.B.K; resources, R.M.AE.; data curation, M.E and A.B.K; writing—original draft preparation, R.M.AE, M.E and A.B.K; writing—review and editing, R.M.AE, M.E and A.B.K; visualization, R.M.AE; supervision, M.E and A.B.K; project administration, M.E and A.B.K; funding acquisition, M.E and A.B.K. All authors have read and agreed to the published version of the manuscript".

Funding: "This research received no external funding"

Conflicts of Interest: "The authors declare no conflict of interest."

Data Availability: The data are available upon reasonable request from the corresponding author.

FOREX Publication
Open Access | Rapid and quality publishing
International Journal of Electrical and Electronics Research (IJEER)
Research Article | Volume 14, Issue 2 | Pages 446-457 | e-ISSN: 2347-470X

REFERENCES

[1] Ayodele, T. R. "Feasibility study of stand-alone hybrid energy system for rural electrification in Nigeria: the case study of Ala-Ajagbusi community." International Journal of Renewable Energy Resources 4.1 (2014): 1-12.

[2] Wei, K., Yang, Y., Zuo, H., & Zhong, D. (2020). A review on ice detection technology and ice elimination technology for wind turbine. Wind Energy, 23(3), 433-457.

[3] Cheng, M.; Zhu, Y. The state of the art of wind energy conversion systems and technologies: A review. Energy conversion and management 2014, 88, 332-347.

[4] Carranza, O.; Figueres, E.; Garcerá, G. ; Gonzalez-Medina, R. Analysis of the control structure of wind energy generation systems based on a permanent magnet synchronous generator. Applied energy 2013, 103, 522-538.

[5] Eriksson, S.; Bernhoff, H. Loss evaluation and design optimisation for direct driven permanent magnet synchronous generators for wind power. Applied Energy 2011, 88(1), 265-271.

[6] Meo, S.; Zohoori, A.; Vahedi, A. Optimal design of permanent magnet flux switching generator for wind applications via artificial neural network and multi-objective particle swarm optimization hybrid approach. Energy Conversion and Management 2016, 110, 230-239.

[7] de Freitas, T. R.; Menegáz, P. J.; Simonetti, D. S. Rectifier topologies for permanent magnet synchronous generator on wind energy conversion systems: A review. Renewable and Sustainable Energy Reviews 2016, 54, 1334-1344.

[8] Yenduri, K.; Sensarma, P. Maximum power point tracking of variable speed wind turbines with flexible shaft. IEEE Transactions on sustainable energy 2016, 7(3), 956-965.

[9] Alnasir, Z.; Kazerani, M. An analytical literature review of stand-alone wind energy conversion systems from generator viewpoint. Renewable and Sustainable Energy Reviews 2013, 28, 597-615.

[10] Hossain, M. M.; Ali, M. H. Future research directions for the wind turbine generator system. Renewable and Sustainable energy reviews 2015, 49, 481-489.

[11] Mohammadpour, H.; Ghassem Zadeh, S.; Tohidi, S. Symmetrical and asymmetrical low-voltage ride through of doubly-fed induction generator wind turbines using gate controlled series capacitor. IET Renewable Power Generation 2015, 9(7), 840-846.

[12] Naidu, N. S.; Singh, B. Experimental implementation of doubly fed induction generator-based standalone wind energy conversion system. IEEE Transactions on Industry Applications 2016, 52(4), 3332-3339.

[13] Schulz, E. M.; Betz, R. E. Use of doubly fed reluctance machines in wind power generation. In 2006 12th International Power Electronics and Motion Control Conference (pp. 1901-1906). IEEE.

[14] Attoui, I.; Omeiri, A. Modeling, control and fault diagnosis of an isolated wind energy conversion system with a self-excited induction generator subject to electrical faults. Energy conversion and management 2014, 82, 11-26.

[15] Nayanar, V., Kumaresan, N., & Gounden, N. G. A. (2016). Wind-driven SEIG supplying DC microgrid through a single-stage power converter. Engineering science and technology, an international journal, 19(3), 1600-1607.

[16] Honsinger, V. B. Steady-state performance of reluctance machines. IEEE Transactions on Power Apparatus and Systems 2007, (1), 305-317.

[17] Abdel-Kader, F. E. The reluctance machine as a self-excited reluctance generator. Electric machines and power systems 1985, 10(2-3), 141-148.

[18] Mohamadein, A. L.; Rahim, Y. H. A., & Al-Khalaf, A. S. Steady-state performance of self-excited reluctance generators. In IEE Proceedings B (Electric Power Applications) 1990,137, (5), pp. 293-298. IEE.

[19] Ogunjuyigbe, A. S. O., Ayodele, T. R., & Adetokun, B. B. Steady state analysis of wind-driven self-excited reluctance generator for isolated applications 2017. Renewable energy, 114, 984-1004.

[20] Alolah, A. I. Capacitance requirements for three phase self-excited reluctance generators. In IEE Proceedings C (Generation, Transmission and Distribution) 1991, 138, (3), 193-198. IEE.

[21] Boldea, I.; Fu, Z. X.; Nasar, S. A. High-performance reluctance generator. In IEE Proceedings B (Electric Power Applications) 1993, 140, (2),124-130. IEE.

[22] Alolah, A. I. Steady-state operating limits of three phase self-excited reluctance generator. In IEE Proceedings C (Generation, Transmission and Distribution) 1992, 139, (3), 261-268. IEE.

[23] Ogunjuyigbe, A. S.; Ayodele, T. R.; Adetokun, B. B. ; Jimoh, A. A. Wind driven self excited reluctance generator for rural electrification. In Wind Turbines-Design, Control and Applications 2016, 231-252. IntechOpen.

[24] Krause, P. C.; Wasynczuk, O.; Sudhoff, S. D.; Pekarek, S. Analysis of electric machinery and drive systems 2002, 2, New York: IEEE press.

[25] Ogunjuyigbe, A. S. O.; Jimoh, A. A.;Nicolae, D. V.;Obe, E. S. Performance analysis of capacitance compensated dual stator winding synchronous reluctance machine. Int Rev Electr Eng 2010,5,437–46.

[26] Novotny, D. W.; Lipo, T. A. Vector control and dynamics of AC drives 1996, Vol. 41. Oxford university press.

[27] Alolah, A. I. Steady-state operating limits of three phase self-excited reluctance generator. In IEE Proceedings C (Generation, Transmission and Distribution) 1992 , 139 (3) , 261-268). IEE.

[28] Su, H., Yang, C., Mdeihly, H., Rizzo, A., Ferrigno, G., & De Momi, ENeural network enhanced robot tool identification and calibration for bilateral teleoperation.2019. IEEE Access, 7, 122041-122051.

International Journal of
Electrical and Electronics Research (IJEER)
Research Article | Volume 14, Issue 2 | Pages 446-457 | e-ISSN: 2347-470X

[29] Braem, D. S., Parrott, N., Hutchinson, L., & Steiert, B. Introduction of an artificial neural network–based method for concentration-time predictions 2022. CPT: Pharmacometrics & Systems Pharmacology, 11(6), 745-754.

[30] Della Krachai, S., Stambouli, A. B., Della Krachai, M., & Bekhti, M. Experimental investigation of artificial intelligence applied in MPPT techniques 2019. International Journal of Power Electronics and Drive Systems, 10(4), 2138.

[31] Khleaf, H. K., Nahar, A. K., & Jabbar, A. S. Intelligent control of DC-DC converter based on PID-neural network 2019. International Journal of Power Electronics and Drive Systems, 10(4), 2254.

[32] Fadzail, N. F., Zali, S. M., Khairudin, M. A., & Hanafi, N. H. Stator winding fault detection of induction generator based wind turbine using ANN 2020. Indonesian Journal of Electrical Engineering and Computer Science, 19(1), 126-133.

[33] Rida, M., Rashad, E. M., El-Samahy, A. A., El-Korfolly, M. I., & Youssef, E. ANN-Based SVC for optimal performance of wind-driven self-excited synchronous reluctance generator 2022. International Journal of Renewable Energy Research, 12, 2082-2091.

[34] Essa, M. E. S. M., Ahmed, A. S., El-Kholy, E. E., & Awad, H. E. S.. MPPT based-ANN for PV Solar-Powered Electric vehicle charging Stations 2025. In 2025 26th International Middle East Power Systems Conference (MEPCON) (pp. 1-7). IEEE.